

1 **Consistent modelling of transport processes and travel times – coupling soil hydrologic**
2 **processes with StorAge Selection functions**

3 **Robin Schwemmler¹ and Markus Weiler¹**

4 ¹Hydrology, Faculty of Environment and Natural Resources, University of Freiburg, Freiburg,
5 Germany

6 Corresponding author: Robin Schwemmler (robin.schwemmler@hydrology.uni-freiburg.de)

7 Key Points:

- 8 • Transport processes and the selection of appropriate StorAge Selection (SAS) functions
9 depend on the considered soil hydrological processes
- 10 • Using a coupled-SAS approach representing advection-dispersion transport by power law
11 distribution function explains the transport of ¹⁸O and bromide in a grassland lysimeter
12 better than other transport representations
- 13 • The complete-mixing transport based on uniform SAS functions and a coarse vertical dis-
14 cretization may lead to errors in tracer arrival
- 15 • Choice between static or time-variant StorAge Selection differently affects parameter sensitivity
16 of hydrologic model and transport model

17 **Abstract**

18 Understanding the transport processes and travel times of pollutants in the subsurface is crucial for
19 an effective management of drinking water resources. Transport processes and soil hydrologic

20 processes are inherently linked to each other. In order to account for this link, we couple the pro-
21 cess-based hydrologic model RoGeR with StorAge Selection (SAS) functions. We assign to each
22 hydrological process a specific SAS function (e.g. power law distribution function). To represent
23 different transport mechanisms, we combined a specific set of SAS functions into four transport
24 model structures: complete-mixing, piston flow, advection-dispersion and advection-dispersion
25 with time-variant parameters. In this study, we conduct modelling experiments at the Rietholzbach
26 lysimeter, Switzerland. All modelling experiments are benchmarked with HYDRUS-1D. We com-
27 pare our simulations to the measured hydrologic variables (percolation and evapotranspiration
28 fluxes and soil water storage dynamics) and the measured water stable isotope signal (^{18}O) in the
29 lysimeter seepage for a period of ten years (1997-2007). An additional virtual bromide tracer ex-
30 periment was used to benchmark the models. Additionally, we carried out a sensitivity analysis
31 and provide Sobol indices for hydrologic model parameters and SAS parameters. Our results show
32 that the advection-dispersion transport model produces the best results. And thus, advective-dis-
33 persive transport processes play a dominant role at Rietholzbach lysimeter. Our modelling ap-
34 proach provides the capability to test hypotheses of different transport mechanisms and to improve
35 process understanding and predictions of transport processes. Overall, the combined model allows
36 a very effective simulation of combined flux and transport processes at various temporal and spa-
37 tial scales.

38 **Plain Language Summary**

39 Knowledge about transport velocities of solutes through the soil is fundamental for an effective
40 protection of drinking water resources from different pollution sources. We subsume transport
41 velocities by the concept of travel times which is time from entering to leaving the soil. The cal-
42 culation of travel times is based on the combination of a model representing the soil-vegetation-

43 atmosphere continuum and model representing the dynamics of solute ages based on probability
44 distributions. The predictive accuracy of our calculations are satisfactory and travel times can be
45 effectively estimated in space and time.

46 **1 Introduction**

47 Understanding the underlying transport processes of solutes, such as nitrate or pesticides, in soils
48 is crucial for an effective management of drinking water resources. Thereby, solute transport and
49 soil hydrologic processes, including percolation of soil water, root water uptake or runoff genera-
50 tion processes, are inherently linked to each other (e.g. Hrachowitz et al., 2016, Sprenger et al.,
51 2019). The quantification of solute transport is still challenging and a unified approach considering
52 flow and transport processes is still missing. Travel times are a widely used concept to enable the
53 quantification of transport processes. They describe the time period of water parcels from entering
54 (e.g. by infiltration) to leaving (e.g. by evapotranspiration, groundwater recharge) a system (e.g.
55 soil). Travel time distributions can inter alia be used to disentangle slow (e.g. transport through
56 soil matrix) from fast transport (e.g. transport through macropores) (Benettin et al., 2015b;
57 Sprenger et al., 2019).

58 In order to simulate water-bound transport of solutes in soil, two types of models can be discerned.
59 On the one hand, physically-based transport models (e.g. Hansen et al., 2012; Köhne et al., 2004;
60 Larsbo and Jarvis, 2005; Sternagel et al., 2019) provide information at high spatial and temporal
61 resolution and important insights into process understanding of solute transport, once they are re-
62 alistically parameterized. However, realistic parameterization requires detailed information on the
63 modelled system (e.g. soil properties), which are usually not available in adequate spatial resolu-
64 tion. Moreover, estimation of solute breakthroughs or travel times requires the application of par-
65 ticle tracking which is computational expensive (e.g Brinkmann et al., 2018). On the other hand,

66 travel-time-based transport models try to include the calculation of travel times in their modelling
67 procedure and the empirical linkage between travel times and solute transport provide useful in-
68 formation about the soil transport patterns. However, they also simplify the transient processes of
69 solute transport in soils. In recent years, travel-time-based transport models using StorAge selec-
70 tion (SAS) functions (Rinaldo et al., 2015) have particularly emerged in solute transport studies
71 (e.g. Asadollahi et al., 2020; Asadollahi et al., 2022; Kumar et al., 2020; Nguyen et al., 2022;
72 Rigon and Bancheri, 2021). They can be distinguished into pure-SAS (e.g. Benettin and Bertuzzo,
73 2018) and coupled-SAS approaches (e.g. Heße et al., 2017). Pure-SAS models rely on measured
74 storage states (e.g. soil water content) and input/output fluxes (e.g. streamflow) and represent un-
75 derlying hydrologic processes in a lumped way, whereas coupled-SAS models link simulated
76 fluxes and storages from hydrologic models with SAS functions. A prerequisite for coupled-SAS
77 models is an appropriate model structure, i.e. a model structure that contains all relevant hydro-
78 logical processes of the considered hydrological system. Unlike pure-SAS models, coupled-SAS
79 models only require a upper boundary condition (e.g. precipitation, potential evapotranspiration)
80 and can be applied as lumped (e.g. Hrachowitz et al., 2013) or spatially-distributed predictions
81 (e.g. Jing et al., 2020).

82 Since Botter et al. (2011) has introduced the master equation, pure-SAS models have widely been
83 applied at the plot scale (e.g. Asadollahi et al., 2020; Asadollahi et al., 2022; Queloz et al., 2015)
84 and catchment scales (e.g. Benettin et al., 2015a; Benettin et al., 2017; Harman, 2015; Wilusz et
85 al., 2020). Thereby, pure-SAS models successfully reproduced measured solute or stable isotope
86 concentrations in lysimeter seepage or streamflow. Due to spatial heterogeneity, travel times at
87 plot scale derived by pure-SAS models differed from those at catchment scale (Queloz et al., 2015).
88 At the plot-scale, pure-SAS modelling experiments with isotope and flourobenzol tracers modeled

89 found that tracer transport is realistically explained if soil water percolation was dominated by old
90 water (Asadollahi et al., 2020; Asadollahi et al., 2022; Queloz et al., 2015).

91 In contrast to pure-SAS models, coupled-SAS models were applied mainly applied at the catch-
92 ment scale (e.g. Benettin et al., 2017; Jing et al., 2020; Kumar et al., 2020; Nguyen et al., 2022;
93 Yang et al., 2019) to predict conservative (e.g. deuterium) and non-conservative solute transport
94 (e.g. nitrate). In these studies, simulations were compared to measured concentrations at the catch-
95 ment outlet. Those integrate all processes and hence only allow for a non-direct, spatially-implicit
96 analysis of internal transport processes (e.g. groundwater recharge). Furthermore, using a non-
97 conservative instead of a conservative tracer blurs the analysis of underlying transport processes
98 due to inherent interaction between transport and biogeochemical processes. To date, coupled-
99 SAS models have neither been applied at the plot scale nor evaluated with plot-scale observations.

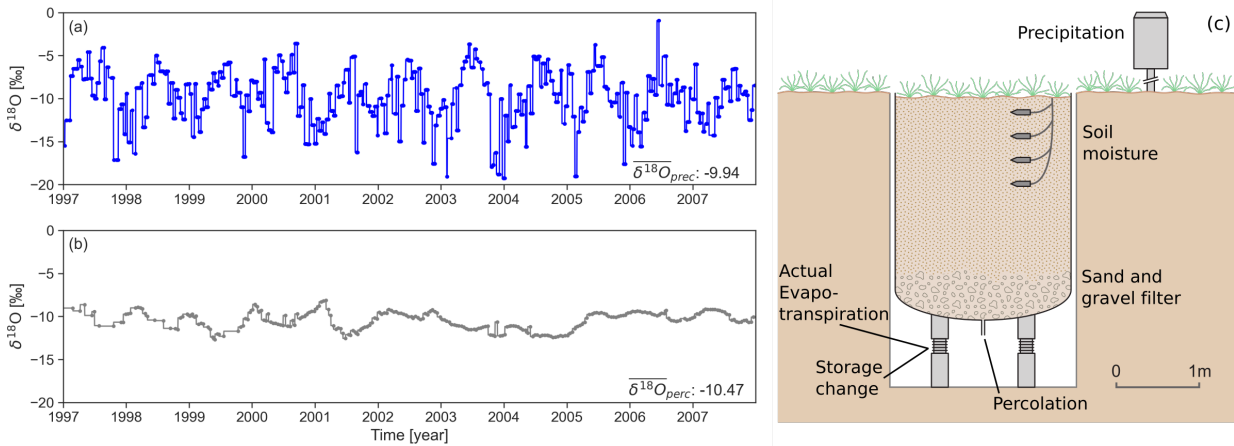
100 In this study, we couple the soil hydrologic model RoGeR (Runoff Generation Research; Stein-
101 brich et al., 2016) with SAS functions. We assign SAS functions to each implemented hydrologic
102 process and test different transport hypotheses (e.g. piston, advection-dispersion) represented by
103 different model structures, each evaluated by a sensitivity analysis using the Sobol method. We
104 use bromide and isotope data from the Rietholzbach lysimeter in Switzerland (Menzel and De-
105 muth, 1993; Seneviratne et al., 2012b). Similar to other studies investigating travel times at the
106 plot scale (e.g. Asadollahi et al., 2020; Sprenger et al., 2016), we provide a benchmark comparison
107 with HYDRUS-1D.

108 We will address three main research questions: (i) What are the sensitivities of hydrologic model
109 parameters and SAS parameters for the different transport model structures using a coupled-SAS

110 approach? (ii) Which transport model structure explains isotope and bromide transport at the Ri-
111 etholzbach lysimeter most realistically? (iii) What are the advantages of a coupled-SAS transport
112 model compared to a physically-based transport model?

113 **2 Study site**

114 The Rietholzbach lysimeter is situated within the pre-alpine Rietholzbach research catchment,
115 Switzerland (Hirschi et al., 2017; Seneviratne et al., 2012b). The lysimeter is located at an eleva-
116 tion of 755 m above sea level and climatic characteristics can be summarized by an average air
117 temperature of 7.1 °C, average annual precipitation of 1459 mm and annual actual evapotranspi-
118 ration of 560 mm. The weightable lysimeter container is filled with the local gleyic cambisol and
119 has an entire depth of 2.5 m (Figure 1). A 0.5 m thick layer of sand and gravel at the bottom of the
120 lysimeter enables free drainage. The 3.14 m² lysimeter surface is covered by grass, which is cut at
121 similar times as the surrounding grassland. We use hydrometeorological data and bi-weekly bulk
122 samples of the stable water isotope oxygen-18 ($\delta^{18}\text{O}$) in precipitation and lysimeter seepage from
123 Seneviratne et al. (2012b). Data gaps in $\delta^{18}\text{O}$ of precipitation have been filled with data from
124 nearby GNIP station St. Gallen (GNIP, 2023) and using PISO.AI (Nelson et al., 2021). Additional
125 model evaluation was possible by including data from a bromide tracer experiment (Menzel and
126 Demuth, 1993) carried out from November 1991 to February 1993. Due to data availability, our
127 study investigates bromide transport the period from November 1991 to February 1993 (see Sect.
128 3.4) and bromide and ^{18}O transport for the period from January 1997 to December 2007 (see Figure
129 1).



130

131 **Figure 1.** (a) Bi-weekly measured $\delta^{18}\text{O}$ in precipitation and (b) measured $\delta^{18}\text{O}$ in lysimeter seepage at Rietholzbach lysimeter. (c)
 132 Cross-section of Rietholzbach lysimeter with measured variables (modified from Seneviratne et al. (2012b)). Storage change and
 133 actual evapotranspiration are derived from measured lysimeter weight change. Air temperature and global radiation were measured
 134 at the nearby are measured at the nearby weather station (not shown).

135 3 Methods

136 3.1 Representation of soil hydrologic processes using the hydrologic model RoGeR

137 As stated above, realistic process-oriented hydrological modelling should be the prerequisite for
 138 successful coupled-SAS approaches. Here, we use the RoGeR model (Steinbrich et al., 2016),
 139 which was developed from the soil hydrological model IN³M (Weiler, 2005) to calculate hydro-
 140 logic fluxes and storage volumes. These fluxes and storage volumes were then coupled with the
 141 SAS functions. In RoGeR, hydrologic fluxes and storage dynamics are simulated with an adapted
 142 temporal resolution (time steps of 10 minutes for high rainfall intensities, hourly time steps for low
 143 rainfall intensities or snow melt, and daily time steps for dry periods). The model requires precip-
 144 itation (mm/10 minutes), daily air temperature ($^{\circ}\text{C}$) and daily potential evapotranspiration
 145 (mm/day) data as input. We corrected the original precipitation data according to Richter (1995)
 146 to account for systematic errors due to wind uncercatch in the measurement of precipitation. Po-

147 tential evapotranspiration is calculated after Makkink (Makkink, 1957) with daily average air tem-
148 perature ($^{\circ}\text{C}$) and daily average global radiation (MJ/m^2). Model parameters are listed in Table 1.

149 The hydrologic processes considered in this study are summarizes as:

150 - **Surface water storage:** Surface water storage comprises an interception storage. Storage pa-
151 rameters are land cover specific and seasonally time-variant.

152 - **Soil water storage:** Soil water storage is divided into an upper (i.e. root zone) and lower
153 storage (i.e. subsoil). Soil hydraulic parameters are derived using a Brooks-Corey scheme
154 (Brooks and Corey, 1966). The two soil storage layers have the same soil hydraulic param-
155 terization.

156 - **Evapotranspiration:** Evapotranspiration is limited by energy (i.e. potential evapotranspira-
157 tion) and water availability (i.e. soil water content). Evapotranspiration occurs sequentially
158 from top to bottom (interception evaporation, soil evaporation and transpiration). Soil evapo-
159 ration is represented by the Stage I – Stage II scheme (Or et al., 2013). Transpiration (i.e. flux
160 by root water uptake) is limited to vegetation/land cover specific root depth. The seasonal
161 variation of ground cover (e.g. deciduous trees) are quantified by a transpiration coefficient.

162 - **Interception:** Interception storage is represented by a single bucket. Liquid and solid precip-
163 itation fill the storage and the interception storage spills over if storage exceeds total storage
164 capacity. Evaporation empties the interception storage.

165 - **Snow accumulation/Snow melt:** Solid precipitation (air temperature below 0°C) accumu-
166 lates in the interception storage or at the ground surface. Snow melt is calculated by a degree-
167 day approach and by a delayed release of melt water.

168 - **Infiltration:** Water infiltrates into the soil matrix, into macropores or shrinkage cracks. Matrix
169 infiltration is implementend by a modified Green-Ampt approach (Green and Ampt, 1911;

170 Peschke, 1985). Infiltration through macropores is represented by the approach from Weiler
 171 (2005) and requires excess of soil matrix infiltration. Macropore infiltration depends on den-
 172 sity, length of vertical macropores and saturated hydraulic conductivity. Depending on the
 173 parameterization, macropore infiltration can attain shares up to 70 % of total infiltration. In-
 174 filtration through shrinkage cracks is adopted from Steinbrich et al. (2016) and depends on
 175 clay and soil water content. Water exchange from macropores/cracks is realized with a ge-
 176 ometry-dependend solution of horizontal infiltration by a Green-Ampt approach (Steinbrich
 177 et al., 2016)

178 **Table 1.** Hydrologic model parameters, their lower and upper parameter boundaries for the Monte-Carlo (MC) sampling and Salt-
 179 elli (SA) sampling, and the final parameter sets of the best 100 simulations (average \pm standard deviation). Usable porosity, fraction
 180 of large pores and fraction of fine pores are auxillary parameters used to set meaningful parameters for air capacity of soil and and
 181 plant available field capacity.

Hydrologic model parameter	Unit	Parameter boundaries		Best parameter(s)
		MC	SA	
Land use/Land cover	lu_id	-	8	8
Makkink coefficient	c1 _{PET}	- 0.55 - 0.65	0.5 - 0.7	0.61 \pm 0.03
Makkink coefficient	c2 _{PET}	mm day ⁻¹ -0.2 - 0.0	-0.4 - 0.2	-0.09 \pm 0.05
Density of vertical macropores	ρ_{mpv}	m ⁻² 10 - 300	1 - 400	202 \pm 70
Length of vertical macropores	l _{mpv}	mm 50 - 1500	1 - 2000	879 \pm 165
Soil depth	z _{soil}	mm	2200	2200
Effective porosity ¹	θ_{eff}	-	0.15 - 0.35	0.21 \pm 0.04
Fraction of large pores	f _{lp}	-	0.1 - 0.6	0.59 \pm 0.05
Fraction of fine pores	f _{fp}	-	1 - f _{lp}	0.41 \pm 0.05
Air capacity of soil	θ_{ac}	-	$\theta_{eff} \cdot f_{lp}$	0.13 \pm 0.03
Plant available field capacity of soil	θ_{ufc}	-	$\theta_{eff} \cdot f_{fp}$	0.09 \pm 0.02
Permanent wilting point of soil	θ_{pwp}	-	0.15 - 0.25 0.1 - 0.25	0.2 \pm 0.03
Saturated hydraulic conductivity of soil	k _s	mm h ⁻¹	5 - 150	83.3 \pm 43.6
Hydraulic conductivity of bedrock	k _f	mm h ⁻¹	2500	2500

182 ¹describes the total volume of mobile soil water storage

- 183 - **Surface runoff:** Surface runoff is generated either by Hortonian (HOF; i.e. infiltration excess)
 184 or saturation overland flow (SOF; i.e. saturation of soil storage).
- 185 - **Capillary rise / Percolation:** Vertical drainage and upward water movement is described by
 186 the approach of Salvucci (1993). For this study, we implemented a free drainage for the lower
 187 boundary condition by setting the hydraulic conductivity of bedrock (k_f) to a constant value
 188 of 2500 mm/h (Table 1).

189 For detailed process and parameter descriptions including all model equations, we refer to the
 190 supporting information or to Schwemmler (2023) for most current information.

191 We run Monte Carlo simulations with 30 000 samples in predefined boundaries (see Table 1).
 192 Initial soil water content was set to field capacity. A multi-objective metric E_{multi} serves to identify
 193 the best performing parameter set.

$$194 \quad E_{multi} = 0.4 KGE_{ET} + 0.2 KGE_{\Delta S} + 0.4 KGE_{PERC} \quad (1)$$

195 where KGE_{ET} is the Kling-Gupta efficiency of evapotranspiration fluxes, $KGE_{\Delta S}$ is the Kling-
 196 Gupta efficiency of total storage change and KGE_{PERC} is the Kling-Gupta efficiency of percolation
 197 fluxes. E_{multi} ranges between 1 and ∞ in which $E_{multi} = 1$ indicates a perfect agreement between
 198 observations and simulations. KGE_{ET} and KGE_{PERC} are assigned with greater weights due to longer
 199 coverage of observed values. The best 100 hydrological simulations are coupled with SAS func-
 200 tions by an offline-scheme (i.e. hydrologic response and hydrologic transport are not simulated
 201 simultaneously).

202 **3.2 Representation of transport processes using StorAge Selection (SAS) functions**

203 We use the fractional SAS function type (fSAS; van der Velde et al., 2012) and solve the SAS
 204 functions for each hydrologic flux Q :

$$205 \quad \tilde{p}_Q(T, t) = \frac{\partial}{\partial T} \Omega_Q(P_S(T, t), t) \quad (2)$$

206 with

$$207 \quad P_S(T, t) = \frac{S_T(T, t)}{S(t)} \quad (3)$$

208 where T is the water age, t is the time step, $\tilde{p}_Q(T, t)$ is the backward travel time distribution of a
 209 specific hydrologic flux, $\omega_Q(T, t)$ is the probability distribution function of the hydrologic flux
 210 (where $\Omega_Q(T, t)$ is the cumulative probability distribution function), $S_T(T, t)$ is the cumulative age-
 211 ranked storage (mm), $S(t)$ is the soil water content (mm) and $P_S(T, t)$ is the cumulative probability
 212 distribution of the storage (where $p_S(T, t)$ is the probability distribution). The hydrologic processes
 213 sequentially update $S_T(T, t)$ at time step t by looping over internal substeps n ($n=6$):

$$214 \quad S(T, i + 1) = S(T, i) \pm \tilde{p}_Q(T, i) \cdot Q(t) \cdot h \quad (4)$$

215 where i is the substep, h is the time increment of the substep (day) and $Q(t)$ (mm day⁻¹) is the flux
 216 from the corresponding hydrologic process. The hydrologic processes update $S_T(T, t)$ in the follow-
 217 ing sequence: infiltration (1; *inf*), soil evaporation (2; *evap_{soil}*), transpiration (3; *transp*), root zone
 218 percolation (4; *perc_{rz}*), subsoil percolation (5; *perc_{ss}*) and capillary rise from subsoil into root zone
 219 (6; *cpr_{rz}*). When the soil surface is covered by snow, we fully mix $\delta^{18}\text{O}$ in precipitation with $\delta^{18}\text{O}$
 220 in the snow cover (Seeger and Weiler, 2014). The $\delta^{18}\text{O}$ in the snow cover might infiltrate while
 221 snow melt.

222 Tracer concentrations (‰ for $\delta^{18}\text{O}$; mg l⁻¹ for bromide) are for each hydrologic flux Q are calcu-
 223 lated as:

$$224 \quad C_Q = \int_{T=0}^{\infty} C_S(T, t) \cdot \alpha_p \cdot \tilde{p}_Q(T, t) dT \quad (5)$$

225 where $C_S(T, t)$ is the age-ranked tracer storage and α_p is the partition coefficient which ranges from
 226 0 (not dissolved) to 1 (fully dissolved). For $\delta^{18}\text{O}$ transport α_p is set to 1. For bromide transport, we

227 set α_p to a value of 0.8 since Menzel and Demuth (1993) found a bromide recovery rate of 80 %,
 228 which could be related to uptake by vegetation or sorption processes. Isotopic fractionation is not
 229 considered owing to the small difference between the average of $\delta^{18}\text{O}$ in precipitation and $\delta^{18}\text{O}$ in
 230 lysimeter seepage (see Figure 1).

231 The age preference of SAS functions and thus the shape of the travel time distribution (TTD) is
 232 controlled by the choice of the probability distribution function. By assigning a probability distri-
 233 bution function as a SAS function to each hydrologic process, we can conceptualize the underlying
 234 transport process. For example, faster transport may be represented by right-skewed ω_Q and slower
 235 transport by left-skewed ω_Q .

236 In order to test different hypotheses about the tracer transport processes at the Rietholzbach lysim-
 237 eter, we group combinations of ω_Q according to four transport model structures. Within these
 238 transport model structures, we represent potential transport processes by specific parameters for
 239 ω_Q (Figure 3):

240 - **Complete-mixing model (CM):** All processes have no age preference (i.e. are well mixed).

241 Each process uses a uniform SAS function:

$$242 \quad \Omega_Q(T, t) = P_s(T, t) \quad (6)$$

243 - **Advection-Dispersion model (AD):** Transport processes of transpiration and percolation are

244 implemented by an advective-dispersive scheme using a power law distribution function:

$$245 \quad \Omega_Q(T, t) = P_s(T, t)^{k_Q} \quad (7)$$

246 Soil evaporation and capillary rise prefer youngest water and are described by advective
 247 transport using a constant parameter k_Q ($k_Q=0.1$; see equation (7)).

248 - **Advection-Dispersion model with time-variant parameters (AD-TV):**

249 Soil evaporation and capillary rise are described as in AD. But transpiration has time-variant
 250 preference implemented by a power law distribution function with a time-variant parameter
 251 k_Q :

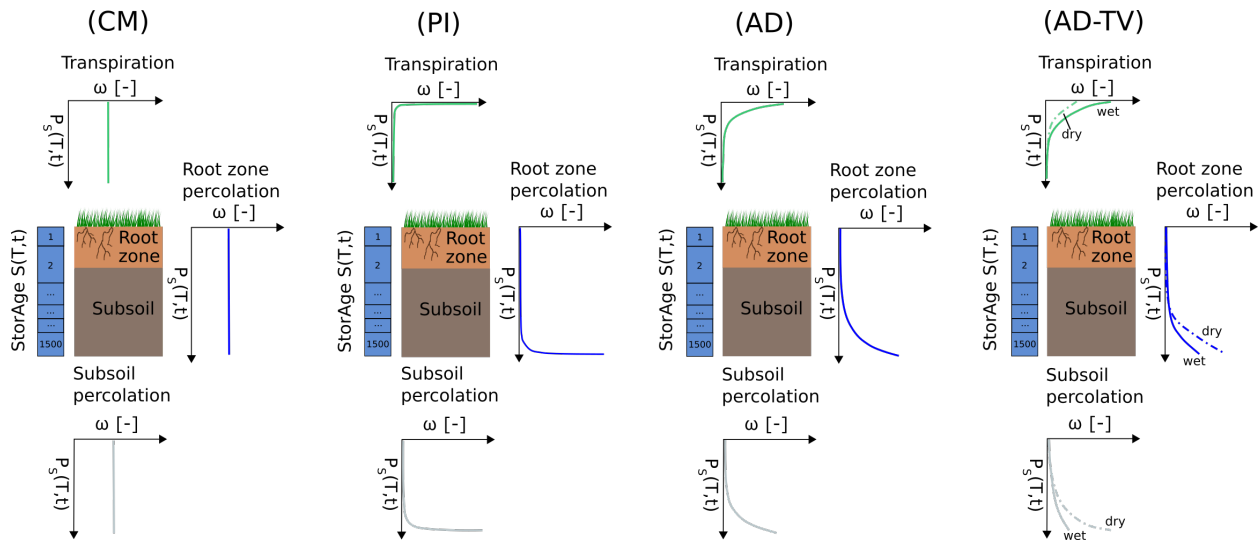
$$252 \quad \Omega_Q(T, t) = P_s(T, t)^{k_Q}, \quad k_Q = c_{1-Q} + c_{2-Q} \frac{S(t) - S_{pwp}}{S_{sat} - S_{pwp}} \quad (8)$$

253 where S_{sat} is the soil storage volume at saturation (mm) and S_{pwp} is the soil storage volume at
 254 permanent wilting point (mm). In equation (8), preference for younger water increases for wet
 255 conditions and decreases for dry conditions.

256 The time-variant preference of percolation is formulated as:

$$257 \quad \Omega_Q(T, t) = P_s(T, t)^{k_Q}, \quad k_Q = c_{1-Q} + c_{2-Q} \left(1 - \frac{S(t) - S_{pwp}}{S_{sat} - S_{pwp}}\right) \quad (9)$$

258 As a result, preference for older water increases for dry conditions and decreases for wet con-
 259 ditions.



260
 261 **Figure 2.** Transport model structures coupled with hydrologic simulations: Complete-mixing transport model (CM), Piston
 262 transport model (PI), Advection-dispersion transport model (AD) and Advection-dispersion transport model with time-variant
 263 SAS parameters (AD-TV). Soil evaporation and capillary rise (not shown) prefer in all transport model structures the youngest
 264 water (see equations (7) with constant $k_Q=0.1$).

265 **Piston-flow model (PI):** Transport processes are purely advective. The power law distribution
 266 function serves as a SAS function. Processes characterized by flux leaving the storage at the
 267 top have a strong preference for younger (equation (7) with constant $k_Q=0.1$). Processes dom-
 268 inated by bottom fluxes have a strong preference for older water (equation (7) with constant
 269 $k_Q=100$).

270 **Table 2** Transport model parameters and their lower and upper parameter boundaries for the Monte-Carlo (MC) sampling and
 271 Saltelli (SA) sampling. Transp indicates parameters of transpiration process and perc indicates parameters of percolation processes.
 272 There are no MC and SA simulations for parameter-free CM and constant-parameter PI.

Transport model parameter	Unit	Transport model structure	Parameter boundaries		Best parameter
			MC	SA	
No parameters		CM	-	-	-
Constant parameters		PI	-	-	-
k_{transp}	-	AD	0.2 - 1	0.1 - 5	0.18
$k_{perc-rz}$	-	AD	1 - 5	0.1 - 5	2.54
$k_{perc-ss}$	-	AD	1 - 5	0.1 - 5	2.08
$c_{1-transp}$	-	AD-TV	0.1 - 0.5	0.1 - 5	-
$c_{2-transp}$	-	AD-TV	0.1 - 2	0.1 - 5	-
$k_{1-transp}$	-	AD-TV	$c_{1-transp}$		0.17
$k_{2-transp}$	-	AD-TV	$c_{1-transp} + c_{2-transp}$		0.97
$c_{1-perc-rz}$	-	AD-TV	1 - 2	0.1 - 5	-
$c_{2-perc-rz}$	-	AD-TV	0.1 - 3	0.1 - 5	-
$k_{1-perc-rz}$	-	AD-TV	$c_{1-perc-rz}$		1.83
$k_{2-perc-rz}$	-	AD-TV	$c_{1-perc-rz} + c_{2-perc-rz}$		4.16
$c_{1-perc-ss}$	-	AD-TV	1 - 2	0.1 - 5	-
$c_{2-perc-ss}$	-	AD-TV	0.1 - 5	0.1 - 5	-
$k_{1-perc-ss}$	-	AD-TV	$c_{1-perc-ss}$		1.66
$k_{2-perc-ss}$	-	AD-TV	$c_{1-perc-ss} + c_{2-perc-ss}$		1.98

273 **3.3 Monte Carlo analysis and sensitivity analysis with the Sobol method**

274 We run Monte Carlo simulations with 10 000 samples. The main purpose of the Monte Carlo
 275 Analysis is the parameter estimation, an additional uncertainty analysis goes beyond this study.
 276 Monte Carlo simulations are computed with the transport model structures AD and AD-TV, but
 277 not with parameter-free CM (see equation (6)) and constant-parameters PI (see equation (7) with

278 $k_Q=0.1$ and $k_Q=100$). Each simulation uses a 5-year simulation period (1997-2001) as a warmup
 279 run (see Figure 1) to derive $C_S(T,t=0)$. After warmup, we rescale $S_T(T,t)$ with $S_{init}/S_T(T,t)$, since we
 280 have knowledge about initial soil water content but do not know initial $\delta^{18}\text{O}$ in soil water. Param-
 281 eter ranges are provided in Table 2. We calculated KGE to evaluate simulations of $\delta^{18}\text{O}$ in perco-
 282 lation. Since $\delta^{18}\text{O}$ in percolation are analyzed from bi-weekly bulk samples, we aggregate simula-
 283 tions to bi-weekly bulk-samples by flux-weighted average.
 284 We additionally conduct a sensitivity analysis using the Sobol method (Saltelli et al., 2008). Pa-
 285 rameter sets are generated using Saltelli's extension of the Sobol sequence (Campolongo et al.,
 286 2011; see Table 1 and Table 2) with a sample size of 1024. We calculate first order and total Sobol
 287 indices for evaluation metrics and age statistics.

288 **3.4 Benchmark comparison to HYDRUS-1D and bromide experiment**

289 Simulations with HYDRUS-1D (Šimůnek et al., 2016, Collenteur et al., 2022) are performed with
 290 a dual-porosity domain. A detailed description of the HYDRUS-1D setup is provided in the sup-
 291 porting information (section S4). We run 30 000 Monte Carlo simulations and select the best per-
 292 forming parameter set based on the multi-objective KGE_{multi} (Sprenger et al., 2016):

$$293 \quad KGE_{multi} = \frac{1}{2} \left(\frac{1}{2} KGE_{\theta} + \frac{1}{2} \left(\frac{1}{2} KGE_{aet} + \frac{1}{2} KGE_{perc} \right) \right) + \frac{1}{2} KGE_{\delta^{18}\text{O}} \quad (10)$$

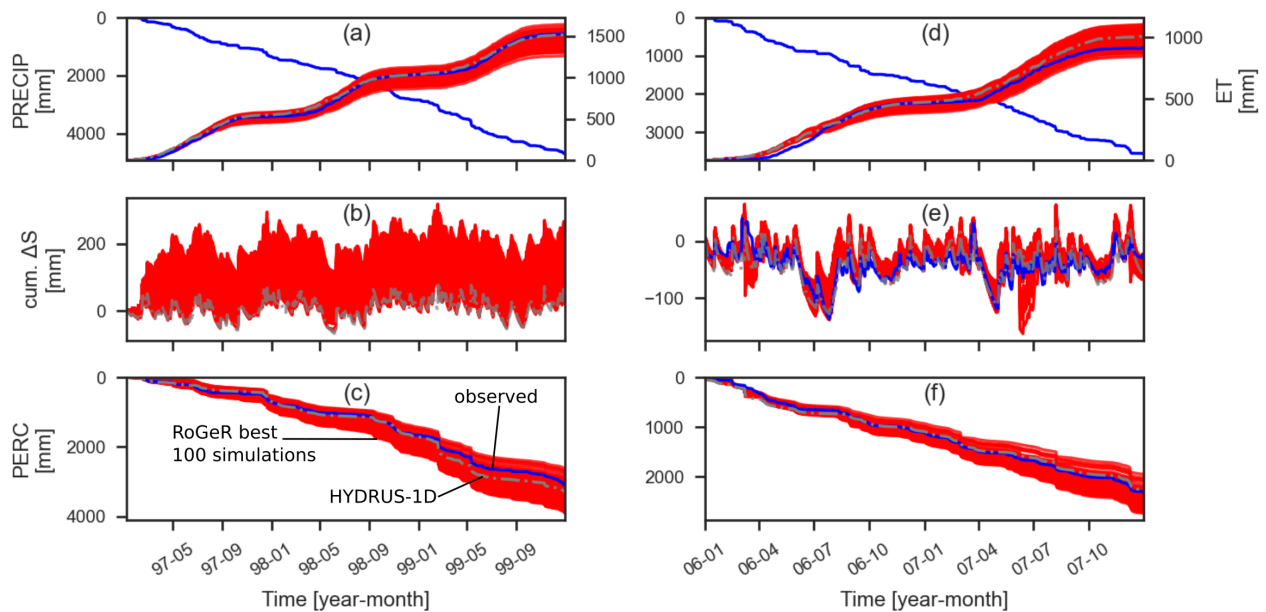
294 where the KGE_{θ} is the average KGE of soil water content at different soil depths z (5 cm, 15 cm,
 295 25 cm 35 cm, 55 cm, 80 cm and 110 cm), KGE_{aet} compares simulated and observed actual evapo-
 296 transpiration, KGE_{perc} compares simulated and observed actual evapotranspiration and $KGE_{\delta^{18}\text{O}}$
 297 compares simulated and observed $\delta^{18}\text{O}$ in percolation.

298 Based on KGE_{multi} (see equation (10)), we select the best performing parameter set and perform
299 three benchmark comparisons between HYDRUS-1D modeling results and RoGeR modeling re-
300 sults:

- 301 1. We compare our results to $\delta^{18}\text{O}$ transport simulations with HYDRUS-1D.
- 302 2. We compare our results to travel time distributions calculated with HYDRUS-1D.
- 303 3. For the virtual bromide experiments, we selected the best performing parameter set (i.e.
304 best $KGE_{\delta^{18}\text{O}}$) for each transport model structure to simulate $\delta^{18}\text{O}$ transport. We, then,
305 transfer the $\delta^{18}\text{O}$ model parameters to the bromide model. Bromide breakthrough is simu-
306 lated with each transport model structure and compared to the results of Menzel and De-
307 muth (1993) and bromide transport simulations with HYDRUS-1D. Since the bromide ex-
308 periment was conducted on 12th November 1991 prior to the time period of our study and
309 the available meteorological input data, we repeat virtual experiments for each year be-
310 tween 1997 and 2006 and inject a bromide mass of 79.9 g (i.e. one mole potassium bromide
311 dissolved in one liter water) at 12th November. Additionally, we used meteorologic data
312 from the nearby station MeteoSwiss station St. Gallen (775 m above sea level; 9°24'W
313 47°26'N) to simulate the period of the bromide experiment. We adjusted the precipitation
314 data by rescaling with the average annual precipitation at the Rietholzbach lysimeter and
315 air temperature data to the altitude difference between St. Gallen and Rietholzbach lysime-
316 ter.

317 **4 Results**318 **4.1 Simulated hydrologic fluxes and storages**

319 The best 100 hydrologic parameters according to E_{multi} (see equation (1)) are summarized in Table
 320 1. The corresponding values of E_{multi} and its metric terms are displayed in Table 3. Values for E_{multi}
 321 are larger for simulations with RoGeR than for simulations with HYDRUS-1D. E_{multi} of simula-
 322 tions with RoGeR show an increasing tendency from drier to wetter antecedent conditions. The
 323 cumulated values of the best 100 simulations according to E_{multi} are compared with observed values
 324 and the best HYDRUS-1D simulation. The comparison for two time periods with highest con-
 325 sistent coverage of observations is shown in Figure 5. Despite a low variance of E_{multi} (see Table
 326 3), simulations reveal differences in the cumulated flux volumes. In particular, absolute differences
 327 are greatest for percolation (Figure 5c and 5f).



328 **Figure 3.** Cumulative precipitation, cumulative simulated and observed evapotranspiration (a,d), cumulative simulated and observed
 329 storage change (b,e), and cumulative simulated and observed percolation (c,f). Data for observed storage change from 1997
 330 to 1999 is not available.

332 **Table 3.** Evaluation metrics of best 100 RoGeR simulations (average \pm standard deviation) and best HYDRUS-1D simulation for
 333 different antecedent soil moisture conditions. Antecedent soil moisture conditions are defined by 10th (θ_{a10}) and 90th (θ_{a90}) percen-
 334 tiles of average observed soil moisture from previous 5 days (θ_a ; dry: $\theta_a < \theta_{a10}$; normal: $\theta_{a10} \leq \theta_a \leq \theta_{a90}$; wet: $\theta_a > \theta_{a90}$)

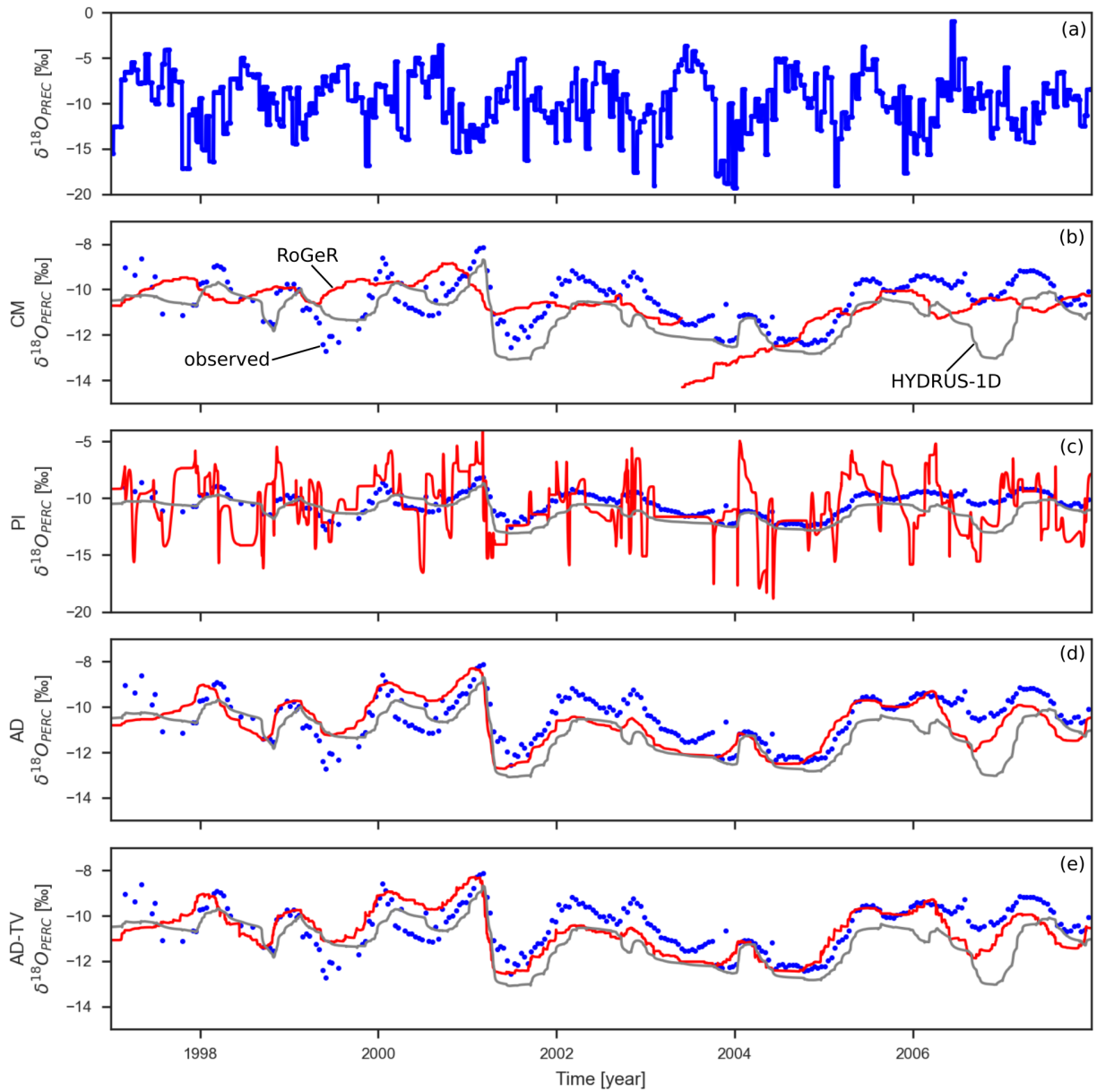
	KGE_{aet}		KGE_{Δs}		KGE_{perc}		E_{multi}	
	RoGeR	HYDRUS-1D	RoGeR	HYDRUS-1D	RoGeR	HYDRUS-1D	RoGeR	HYDRUS-1D
total	0.78 \pm 0.05	0.80	0.74 \pm 0.1	-0.05	0.53 \pm 0.06	0.58	0.67 \pm 0.02	0.54
dry	0.55 \pm 0.09	0.60	0.83 \pm 0.05	0.59	0.16 \pm 0.1	0.06	0.45 \pm 0.03	0.39
normal	0.79 \pm 0.05	0.81	0.69 \pm 0.1	-0.1	0.43 \pm 0.08	-0.74	0.63 \pm 0.03	0.01
wet	0.81 \pm 0.04	0.88	0.67 \pm 0.13	0.52	0.65 \pm 0.1	0.69	0.72 \pm 0.06	0.73

335 4.2 Monte Carlo analysis

336 The best simulation for $\delta^{18}\text{O}$ in percolation of each transport model structure is shown in Figure 6.
 337 The AD and AD-TV model structure visually agrees with the general pattern of $\delta^{18}\text{O}$ observations
 338 in the percolation flux. The CM-model depicts lower agreement between simulations and obser-
 339 vations, while the PI-model shows the lowest agreement among the four model structures. KGE
 340 values (Table 4) confirm the visual pattern of Figure 6. The AD-model structure scores highest
 341 KGE values and performs slightly better than HYDRUS-1D. We tested further transport model
 342 structures with RoGeR (e.g. preferential transport). For the results of the additional model struc-
 343 tures, we refer to the supporting information (section S2). In contrast to the hydrologic simulations,
 344 the transport simulations from the CM, AD and AD-TV transport model structure picture a de-
 345 crease of model performance from drier antecedent conditions to wetter antecedent conditions.

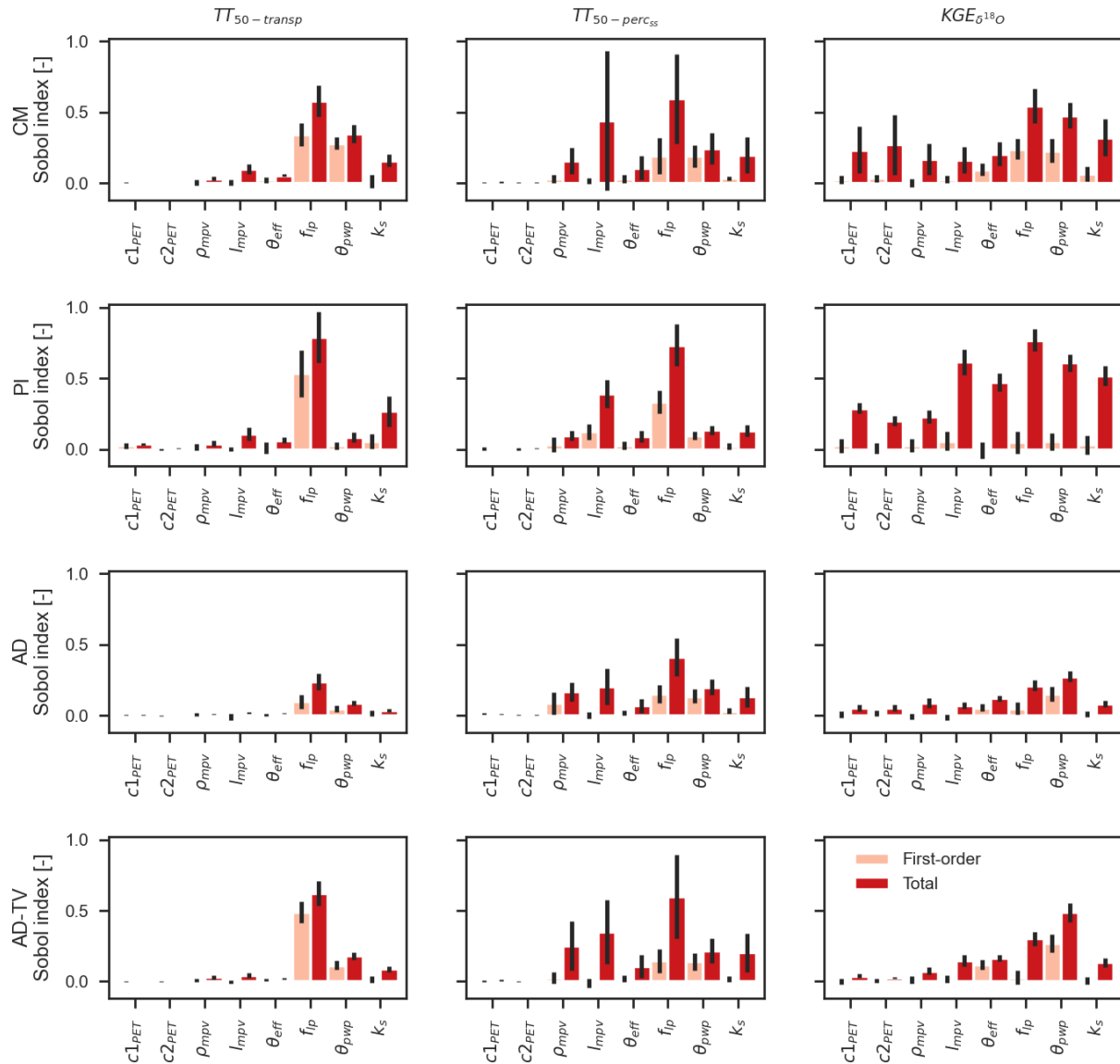
346 4.3 Sensitivity analysis with the Sobol' method

347 Figure 7 shows Sobol' indices of hydrologic model parameters for averaged median travel time of
 348 transpiration ($TT_{50-transp}$) and percolation ($TT_{50-perc}$) and for KGE of $\delta^{18}\text{O}$ in percolation ($KGE_{\delta^{18}\text{O}}$).
 349 The four transport model structures share the same set of sensitive hydrologic model parameters.
 350 For the two travel time statistics, Sobol' indices are greatest for fraction of large pores (f_{lp}) except



351
 352 **Figure 4.** Observed $\delta^{18}\text{O}$ in precipitation (a) and observed and simulated $\delta^{18}\text{O}$ in percolation with RoGeR and HYDRUS-1D (b-
 353 e). Values are shown for different model structures (see Figure 2).

354 for $\text{KGE}_{\delta^{18}\text{O}}$ of AD and AD-TV for which Sobol' indices of permanent wilting point (θ_{pwp}) are
 355 greatest. In addition to that, averaged $TT_{50\text{-perc}}$ is sensitive for macropore parameters (ρ_{mpv} and l_{mpv}).
 356 In general, total Sobol' indices exceed values of first-order Sobol' indices. Total Sobol' indices
 357 describe the fraction of variance that is caused by the variability of the considered parameter. First-



358

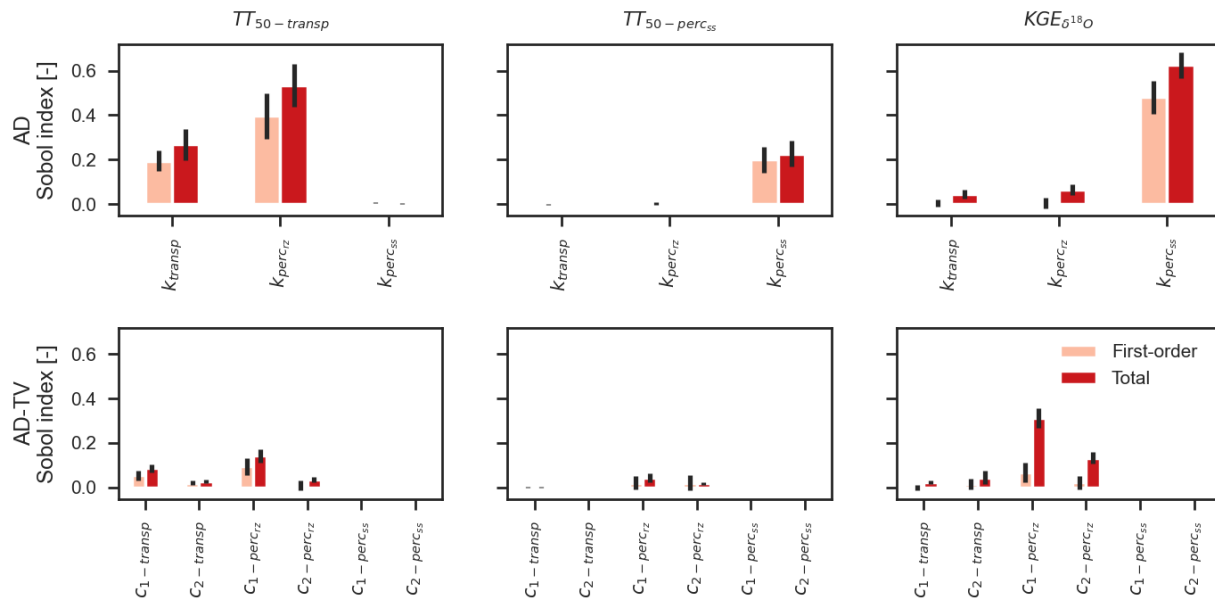
359 **Figure 5.** Sobol' indices with error bars (95% confidence interval) of hydrologic model parameters (see Table 1) calculated for
 360 averaged median travel time of transpiration ($TT_{50-transp}$), averaged median travel time of percolation ($TT_{50-perc_{55}}$) and KGE of $\delta^{18}O$
 361 in percolation ($KGE_{\delta^{18}O}$). Values are shown for complete-mixing transport model structure (CM), piston-flow transport model
 362 structure (PI), advection-dispersion transport model structure (AD) and advection-dispersion transport model structure with time-
 363 variant SAS parameters (AD-TV).

364 order Sobol' indices represent direct contribution to the total Sobol' indices of the considered pa-

365 rameter. A difference between total Sobol' indices and first-order Sobol' indices might be ex-

366 explained by parameter interactions. These differences are more distinct for $TT_{50-perc}$. The gap be-
 367 tween first-order Sobol' indices and total Sobol' indices suggests a strong interaction between
 368 parameters.

369 Sobol' indices of SAS parameters for $TT_{50-transp}$, $TT_{50-perc}$ and $KGE_{\delta^{18}O}$ are displayed in Figure 8.
 370 Comparing the Sobol indices between hydrologic model parameters and SAS parameters reveal
 371 two different results: (i) The AD model structure is more sensitive for SAS parameters than for
 372 hydrologic model parameters. (ii) The AD-TV model structure is more sensitive for hydrologic
 373 model parameters than for SAS parameters. Regarding travel times, we found greater Sobol' indi-
 374 ces for $TT_{50-transp}$ than for $TT_{50-perc}$.



375
 376 **Figure 6.** Sobol' indices with error bars (95% confidence interval) of SAS parameters (see Table 2) calculated for averaged median
 377 travel time of transpiration ($TT_{50-transp}$), averaged median travel time of percolation ($TT_{50-perc}$) and KGE of $\delta^{18}O$ in percolation
 378 ($KGE_{\delta^{18}O}$). Values are shown for advection-dispersion transport model structure (AD) and advection-dispersion transport model
 379 structure with time-variant SAS parameters (AD-TV).

380 **Table 4.** KGE of best $\delta^{18}\text{O}$ simulations for different antecedent soil moisture conditions. Antecedent soil moisture conditions are
 381 defined by 10th (θ_{a10}) and 90th (θ_{a90}) percentiles of average observed soil moisture from previous 5 days (θ_a ; dry: $\theta_a < \theta_{a10}$; normal:
 382 $\theta_{a10} \leq \theta_a \leq \theta_{a90}$; wet: $\theta_a > \theta_{a90}$)

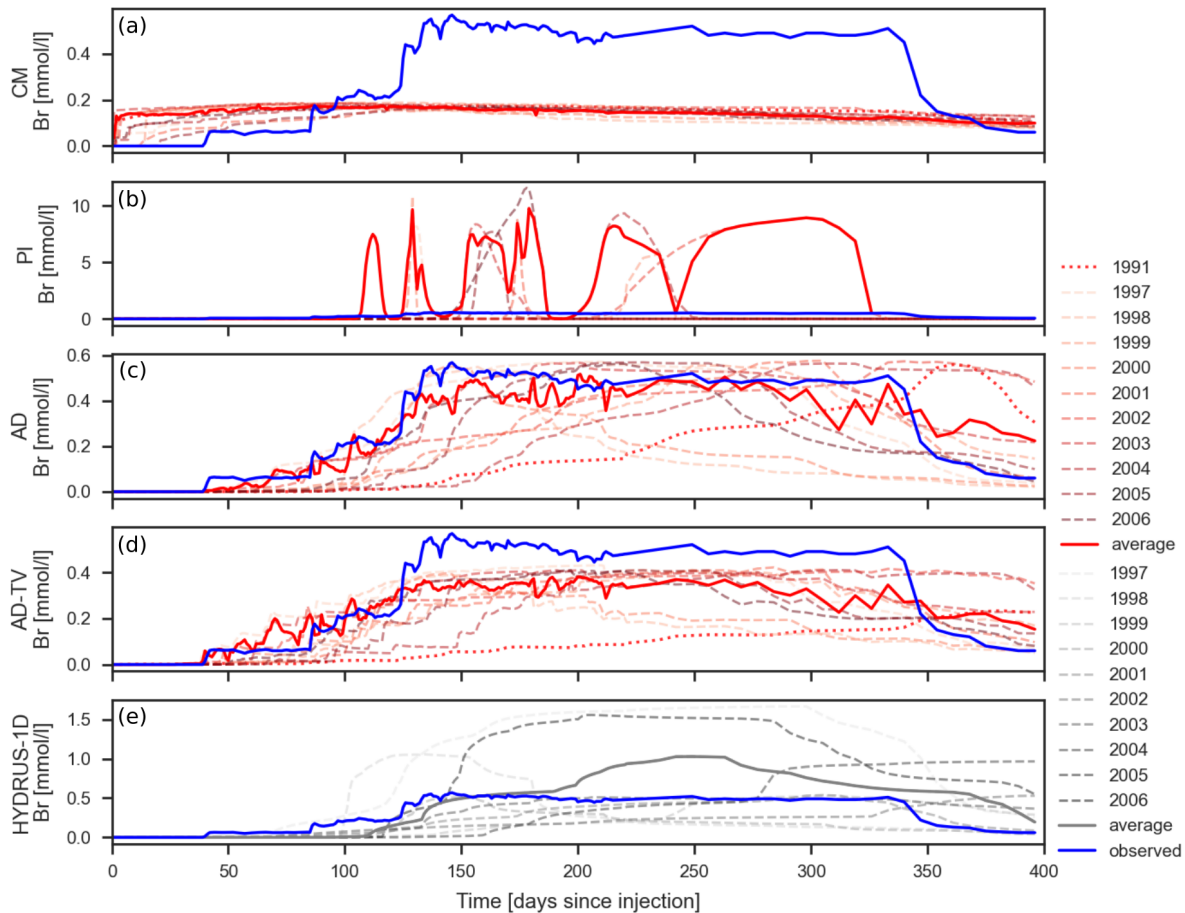
	CM	PI	AD	AD-TV	HYDRUS-1D
total	0.47	-0.37	0.74	0.74	0.68
dry	0.54	0.06	0.78	0.78	0.62
normal	0.47	-0.37	0.73	0.74	0.60
wet	0.31	0.21	0.71	0.71	0.69

383 4.4 Benchmark comparison to virtual bromide experiments and water age statistics of HYDRUS-1D 384 simulations

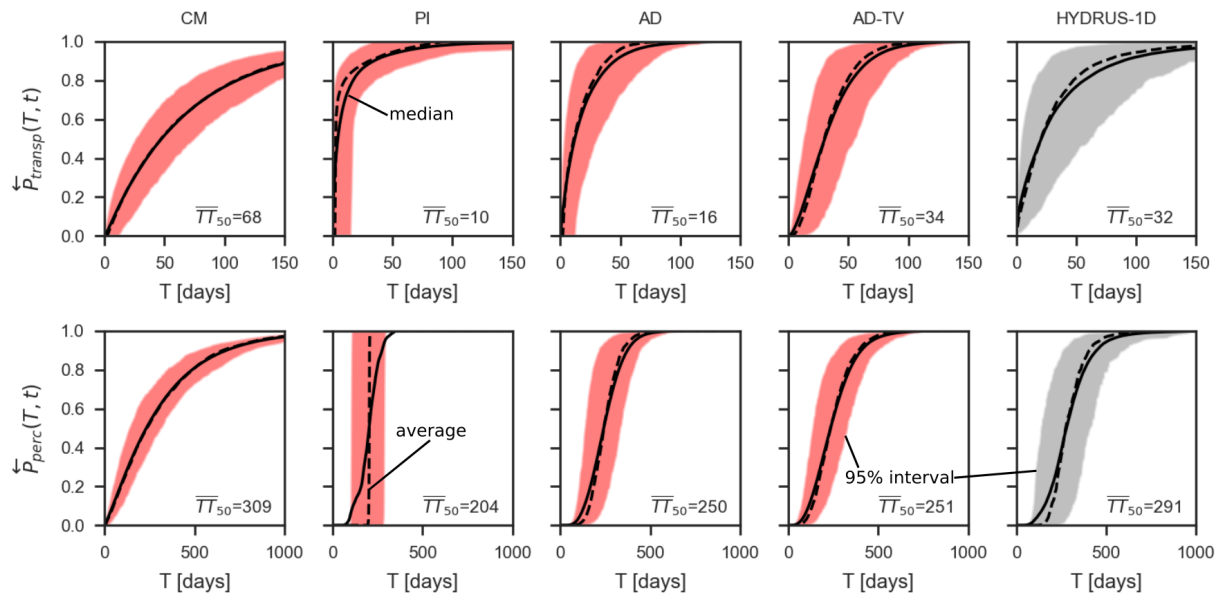
385 Results of virtual bromide experiments are presented in Figure 7. The four model structures predict
 386 different bromide breakthrough curves. We found that bromide breakthrough curves of single vir-
 387 tual experiments deviate from each other due to different meteorological conditions. Furthermore,
 388 single virtual experiments diverge from observed bromide breakthrough curves. For example, the
 389 drought in year 2003 causes a late arrival of the bromide pulse. However, the average breakthrough
 390 curves produced by AD and AD-TV are similar and the average breakthrough curves agree well
 391 in terms of timing and magnitude with the observed bromide breakthrough curve. The average
 392 bromide breakthrough curves derived from CM and PI are different. In particular, CM simulates
 393 bromide breakthrough too early. PI simulates bromide breakthrough too late and the magnitude of
 394 the breakthrough is strongly overestimated.

395 The comparison between the backward travel time distributions calculated with the four transport
 396 model structures and HYDRUS-1D is depicted in Figure 8. Again, backward travel time distribu-
 397 tions calculated by CM and PI are different to the backward travel time distributions calculated by
 398 AD, AD-TV and HYDRUS-1D. Especially travel times computed with CM extend to a wider
 399 range of water ages than the other models. While backward travel time distributions of percolation

400 derived from AD, AD-TV and HYDRUS-1D are similar, backward travel time distributions of
 401 transpiration estimated by AD, AD-TV and HYDRUS-1D reveal differences. AD-TV estimates
 402 older travel times for transpiration than AD. Transpiration travel times from HYDRUS-1D cover
 403 a wider range of water ages and the tails are older.



404
 405 **Figure 7.** Bromide breakthrough curves from virtual bromide experiments and observed bromide breakthrough curve (modified
 406 from Menzel and Demuth (1993)). 79.9 g of bromide has been injected at 12th November of each year. Average values are weighted
 407 by bromide mass of percolation. Simulations are shown for complete-mixing transport model structure (a; CM), piston-flow
 408 transport model structure (b; PI), advection-dispersion transport model structure (c; AD), advection-dispersion transport model
 409 structure with time-variant SAS parameters (d; AD-TV) and HYDRUS-1D with dual-porosity domain (e; HYDRUS-1D).



410

411 **Figure 8.** Simulated backward travel time distributions of transpiration and percolation. Averaged median travel times (in days)

412 are displayed in the right bottom corner.

413 **5 Discussion**414 **5.1 Sensitive parameters for travel time statistics and model accuracy**

415 The sensitivity analysis using the Sobol method for the coupled RoGeR model with SAS functions

416 revealed different sensitivities for the RoGeR-AD and RoGeR-AD-TV model structure (Figures 6

417 and 7). The results for a static SAS parameterization imply that travel time estimates and predictive

418 model accuracy are similarly affected by parameters of the hydrologic model and SAS functions.

419 When using a time-variant SAS parameterization, hydrologic model parameters have a greater

420 impact than SAS parameters on the results. One reason for this larger sensitivity might be the

421 dependency from the soil water content (see equations (8) and (9)) on the transport simulations.

422 Despite this difference, RoGeR-AD and RoGeR-AD-TV have in common that parameters related

423 to soil water storage (f_p and θ_{pwp}) have the greatest impact on travel times and model accuracy.

424 The two studies of Menzel and Demuth (1993) and Weiler and Naef (2003) at the Rietholzbach
425 site provided experimental evidence that macropores play an important role for soil water fluxes
426 and tracer transport. The macropore parameters estimated by the Monte Carlo analysis (Table 1)
427 agree well with observations from Weiler and Naef (2003). They found a macropore density of
428 228 m^{-2} compared to the estimated $202 \pm 70 \text{ m}^{-2}$. The sensitivity analysis shows that macropores
429 influence the travel time estimation of percolation, while they have little impact on model accuracy
430 and travel times of transpiration.

431 The closure of the lysimeter solute balance could only be partly constrained since solute (^{18}O)
432 information has only been available at the bottom of the lysimeter. To fully constrain the model
433 would require solute information from soil water and root water uptake (e.g. Asadollahi et al.,
434 2022). As a consequence, age preference of transpiration and sensitive parameters for predictive
435 accuracy of the transpiration process cannot be directly evaluated. For example, the model repro-
436 duces a similar signal of $\delta^{18}\text{O}$ in percolation with a younger age preference and an older age pref-
437 erence (Figures 2,4, S6 and S7). However, the best SAS parameter of transpiration (Table 2) are
438 consistent with Asadollahi et al. (2020) who found $k=0.2$ for the evapotranspiration process (with-
439 out constrains for evapotranspiration) at another grassland lysimeter.

440 **5.2 Hypothesis-driven modelling of ^{18}O transport and bromide transport**

441 The comparison between observed and simulated $\delta^{18}\text{O}$ in percolation and the virtual bromide ex-
442 periments proved that SAS parameters which can be linked to an advective-dispersive transport
443 process can explain ^{18}O transport and bromide transport to a large extent (Figures 4 and 7). How-
444 ever, uniform SAS functions could explain the dampening of the isotope signal well, but not the
445 transport process of a individual tracer signal like the bromide application. The estimated model
446 parameters of the AD models demonstrate a realistic pattern of the conceptualized processes. Since

447 the soil water dynamics are represented by equations which are governed capillary forces, RoGeR
448 enables a bypass flow in the root zone but mobile soil water is ultimately abstracted by the soil
449 matrix and thus leads to a slower transport (i.e. preference for older water with $k_Q > 1$). From
450 capillary-driven perspective, the older age preference ($k_Q > 1$) of percolation processes is physi-
451 cally consistent. However, RoGeR may reach its limits in case of a rapid response. We suppose,
452 that such a rapid response is more important for shallow soils with high connectivity of macropores
453 from the soil surface to the percolation depths. In such cases, it might be more consistent to imple-
454 ment preferential flow through gravity-driven theory (Germann and Prasuhn, 2018). The dye tracer
455 experiments of Weiler and Naef (2003) conducted within the Rietholzbach catchment proved the
456 occurrence of preferential flow at 1 m soil depth. Consequently, age preference of SAS might be
457 younger where macropores exist. In order to test the hypothesis of specific transport with a young
458 water preference, we would need a higher sampling frequency of ^{18}O during events from the ly-
459 simeter seepage and additional soil water samples at different soil depths.

460 The virtual bromide experiments revealed that SAS parameters of advective-dispersive transport
461 estimated with ^{18}O could be successfully transferred to predict bromide breakthrough (Figure 7).
462 The average bromide breakthrough simulated by RoGeR-AD exhibits visually a better agreement
463 than RoGeR-AD-TV or HYDRUS-1D, respectively. The lower agreement of RoGeR-AD-TV
464 might be due to parameter estimation with bi-weekly ^{18}O samples which causes a loss of infor-
465 mation and a better agreement might be feasible with higher sampling frequency of ^{18}O . HY-
466 DRUS-1D cannot predict the first arrival of the solute at the bottom very well, which could be
467 attributed to its capillary-driven model framework. The comparison between individual bromide
468 breakthrough curves demonstrate nicely the impact of different meteorologic conditions on
469 transport velocities. For example, bromide pulse arrives later when injected in a drought year (e.g.

470 year 2003; see Figure S2) whereas bromide pulse arrives earlier when injected under wetter mete-
471 orologic conditions (e.g. year 1998; see Figure S2).

472 A key result of the virtual bromide experiments is that the tracer signals simulated by SAS with a
473 uniform probability distribution function arrive substantially earlier than indicated by the observa-
474 tions (Figure 7). We found a similar pattern for the ^{18}O modelling experiments which support the
475 findings from the virtual bromide experiments. These results clearly demonstrate the consequence
476 of using the complete-mixing assumption for depth-implicit solute transport model (e.g. soil is dis-
477 cretized by 2-3 soil layers). We can support the argumentation in Sternagel et al. (2022) and we
478 suggest going beyond the commonly applied complete-mixing assumption (e.g. Heße et al., 2017;
479 Kumar et al., 2020).

480 Finally, we want to stress several limitations of the hypothesis-driven modelling approach pre-
481 sented in this study. Since evaporative fractionation of ^{18}O has not been implemented into the
482 model framework, evaporative fractionation of ^{18}O should be negligible, which is the case at the Ri-
483 etholzbach lysimeter due to the dense grass cover and site specific climate conditions. Although we
484 account for non-conservative behavior of bromide by considering partitioning of either root water
485 uptake or sorption processes (see equation (5)), the assumption of $\alpha_p=0.8$ might not be transferable
486 to other sites. The non-conservative behavior is important for longer time periods (i.e. longer than
487 the event length; Sternagel et al., 2019) and sorption processes are controlled by clay content of
488 soil and pH-conditions (Groh et al., 2018). We suppose that RoGeR-SAS is limited to deep soils
489 and/or partly structured soils (e.g. macropore network of the soil column is partly connected) for
490 which solute flushing at the event scale are less relevant. For a better representation of solute
491 flushing, it might be worth to implement infiltration and percolation based on gravity-driven theory

492 (Germann and Prasuhn, 2018) and compare it to the approach presented in this study. Such a com-
493 parison should investigate how and when gravity-driven transport is induced. For example, the
494 interplay between rainfall characteristics (e.g. rainfall intensity) or soil properties (e.g. macropore
495 network) may play a decisive role (Demand and Weiler, 2021).

496 **5.3 Coupling simulated hydrologic fluxes and storages with SAS functions**

497 We estimated parameters of HYDRUS-1D with dual-porosity domains using the observed soil
498 water content time series at different soil depth to maximize information for the spatially discrete
499 HYDRUS model (see equation (10)). However, to allow for a fair comparison between RoGeR
500 and HYDRUS-1D, we evaluated the model results with the same metrics (Tables 3 and 4). These
501 results show that RoGeR predicts hydrologic variables in general better than HYDRUS-1D. $\delta^{18}\text{O}$
502 in percolation and bromide breakthrough are reproduced similarly well by RoGeR and HYDRUS-
503 1D (Figures 4 and 7). RoGeR performs slightly better than HYDRUS-1D in terms of $\text{KGE}_{\delta^{18}\text{O}}$ and
504 for predicting the bromide experiment. Furthermore, travel time statistics estimated by RoGeR
505 with advective-dispersive transport and by HYDRUS-1D show similar distributions (Figure 8).
506 The similarities between the two models and the good agreement between simulations with RoGeR
507 and observations confirm the usability of coupling SAS functions with a process-based hydrologic
508 model.

509 Besides that the complete program code used for this study is publicly available and thus fosters
510 reproducibility, another major advantage of RoGeR compared to HYDRUS-1D is that the compu-
511 tation of travel times is approximately 340 times faster. Travel time computation with HYDRUS-
512 1D took 340 hours whereas travel time computation with RoGeR took 1 hour. Comparing the cou-
513 pled-SAS model as presented here with a pure-SAS model (e.g. Benettin and Bertuzzo, 2018) in
514 terms of applicability shows that only data of the upper condition is required rather than measured

515 fluxes of all outflows from the considered hydrologic system. In many cases, such measurements
516 are not available. Another advantage is that RoGeR requires a lower number of parameters. More-
517 over, the model does not rely on complex calibration schemes. Instead, parameters of RoGeR can
518 be derived from available environmental data (e.g. soil maps; Steinbrich et al., 2016) and may
519 readily applied to sites with such datasets. Disadvantages of RoGeR compared to HYDRUS-1D
520 are mainly attributed to the low vertical discretization with two soil layers. HYDRUS-1D provides
521 more information in the vertical dimension (e.g. spatio-temporal tracer distributions in the soil).
522 For example, research questions concerning highly dynamic processes (e.g. depth of root water
523 uptake) can only be obtain with spatially detailed results of HYDRUS-1D.

524 Although data requirements of coupled-SAS models are less strict than for pure-SAS models, a
525 major challenge for coupling SAS functions with simulated hydrologic variables consists of the
526 realistic representation of the considered hydrologic system. We selected the best 100 hydrologic
527 simulations according to a performance metric realized with different parameters and coupled the
528 simulations with SAS functions. All 100 hydrologic model realization coupled with AD and AD-
529 TV were capable to achieve $KGE_{\delta^{18}O} > 0.7$, hence a certain parameter equifinality could not be
530 resolved (Figure S4). For example, values for k_s range from 11.6 to 149.6 mm/h.

531 As already been shown by Asadollahi et al. (2020), we could also confirm that using single-param-
532 eter SAS function is suitable to predict solute leaching within a soil column. Since a dual-param-
533 eter SAS function produced very similar results, the question about the shape of SAS functions
534 (e.g. Heidbüchel et al., 2020) remains open. We suggest to perform a multi-site (e.g. lysimeters
535 with different soil properties, vegetation cover and climatic conditions) comparison including dif-
536 ferent kind of tracer signals (e.g. seasonally varying isotopic signal vs injection of pollution tracers
537 or nutrients at specific time) to further improve our knowledge about SAS-based solute transport.

538 **6 Conclusions**

539 The ^{18}O and bromide transport through a grass covered weighted lysimeter has been extensively
540 investigated using simulations of RoGeR-SAS and HYDRUS-1D with a dual-porosity domain.
541 The simulations with different transport model structures exhibited high sensitivities for parame-
542 ters related to the soil water storages. The two advective-dispersive transport model structures of
543 RoGeR showed particularly different sensitivities depending on the choice between a static or a
544 time-variant SAS parameterization. We further found that the leaching of ^{18}O and bromide can be
545 realistically explained to a large extent by SAS with power law distribution function linked to
546 advective-dispersive transport. The two selected advective-dispersive transport model structures
547 of RoGeR-SAS showed particularly different sensitivities depending on the choice between a static
548 or a time-variant SAS parameterization. Although a uniform SAS resulting in complete-mixing
549 reproduces well the dampening of the ^{18}O percolation signal, this transport assumption leads to a
550 strong temporal mismatch of the tracer signal (i.e. early arriving of tracer signal), if used in
551 transport models with coarse vertical discretization at sites with deep soils. The results of RoGeR-
552 SAS with advective-dispersive transport model structures show very similar results than the more
553 complex HYDRUS-1D model and agrees well with the lysimeter measurements. RoGeR-SAS
554 substantially reduces computational time of travel times but at the cost of a simpler, but more
555 parsimonious vertical discretization. Therefore, the combination of a hydrologic model with
556 SAS function linked to individual fluxes and processes has a great potential to effectively simulate
557 water balance components and the related solute transport at various temporal and spatial scales.
558 The new RoGeR-SAS could also be extended to solutes with more complex transport processes to
559 allow simulations of nutrient cycles or pollutants.

560

561 **Acknowledgments**

562 This research was supported by the Helmholtz Association of German Research Centres through grant no 42-2017.
 563 We are grateful to Jens Lange and Dominic Demand for their constructive comments on the first draft. Jürgen Strub
 564 provided the illustration of the lysimeter and the measured bromide breakthrough curve. We also acknowledge Martin
 565 Hirschi, Dominik Michel and Sonia I. Seneviratne from the Institute for Atmospheric and Climate Science at ETH
 566 Zürich for providing the measurements from the Rietholzbach site, including the stable water isotope measure-
 567 ments, lysimeter data, and meteorological data. The authors acknowledge support by the High Performance and Cloud
 568 Computing Group at the Zentrum für Datenverarbeitung of the University of Tübingen, the state of Baden-Württem-
 569 berg through bwHPC and the German Research Foundation (DFG) through grant no INST 37/935-1 FUGG.

570

571 **Open Research**

572 The code and data used for this project are available at <https://doi.org/10.5281/zenodo.7633362> (Schwemmler, 2023)
 573 and <https://doi.org/10.5281/zenodo.763228>. The observational data used in this project is available from the Land-
 574 Climate Dynamics group (Prof. Sonia Seneviratne) at ETH Zurich (isotope data will be available at
 575 <https://doi.org/10.3929/ethz-b-000596572> (Michel et al., 2023); other Rietholzbach data will be available at
 576 <https://doi.org/10.3929/ethz-b-000596657> (Seneviratne et al., 2012a)).

577

578 **References**

- 579 Asadollahi, M., C. Stumpp, A. Rinaldo, and P. Benettin (2020), Transport and Water Age Dynamics in Soils: A
 580 Comparative Study of Spatially Integrated and Spatially Explicit Models, *Water Resources Research*, 56(3),
 581 e2019WR025539. <https://doi.org/10.1029/2019wr025539>
- 582 Asadollahi, M., M. F. Nehemy, J. J. McDonnell, A. Rinaldo, and P. Benettin (2022), Toward a Closure of
 583 Catchment Mass Balance: Insight on the Missing Link From a Vegetated Lysimeter, *Water Resources Research*,
 584 58(4), e2021WR030698. <https://doi.org/10.1029/2021WR030698>
- 585 Benettin, P., and E. Bertuzzo (2018), tran-SAS v1.0: a numerical model to compute catchment-scale hydrologic
 586 transport using StorAge Selection functions, *Geosci. Model Dev.*, 11(4), 1627-1639. <https://doi.org/10.5194/gmd-11-1627-2018>
- 587 Benettin, P., J. W. Kirchner, A. Rinaldo, and G. Botter (2015a), Modeling chloride transport using travel time
 588 distributions at Plynlimon, Wales, *Water Resources Research*, 51(5), 3259-3276.
 589 <https://doi.org/10.1002/2014WR016600>
- 590 Benettin, P., C. Soulsby, C. Birkel, D. Tetzlaff, G. Botter, and A. Rinaldo (2017), Using SAS functions and high-
 591 resolution isotope data to unravel travel time distributions in headwater catchments, *Water Resources Research*,
 592 53(3), 1864-1878. <https://doi.org/10.1002/2016WR020117>
- 593 Benettin, P., S. W. Bailey, J. L. Campbell, M. B. Green, A. Rinaldo, G. E. Likens, K. J. McGuire, and G. Botter
 594 (2015b), Linking water age and solute dynamics in streamflow at the Hubbard Brook Experimental Forest, NH,
 595 USA, *Water Resources Research*, 51(11), 9256-9272. <https://doi.org/10.1002/2015WR017552>
- 596 Botter, G., E. Bertuzzo, and A. Rinaldo (2011), Catchment residence and travel time distributions: The master
 597 equation, *Geophysical Research Letters*, 38(11). <https://doi.org/10.1029/2011GL047666>
- 598 Brinkmann, N., S. Seeger, M. Weiler, N. Buchmann, W. Eugster, and A. Kahmen (2018), Employing stable isotopes
 599 to determine the residence times of soil water and the temporal origin of water taken up by *Fagus sylvatica* and
 600 *Picea abies* in a temperate forest, *New Phytol.*, 219(4), 1300-1313. <https://doi.org/10.1111/nph.15255>
- 601 Brooks, R. H., and A. T. Corey (1966), Properties of porous media affecting fluid flow, *Journal of the Irrigation and*
 602 *Drainage Division*, 92(2), 61-90.
- 603 Campolongo, F., A. Saltelli, and J. Cariboni (2011), From screening to quantitative sensitivity analysis. A unified
 604 approach, *Comput Phys Commun*, 182(4), 978-988. <https://doi.org/10.1016/j.cpc.2010.12.039>
- 605 Collenteur, R. A., G. Brunetti, and M. Vremec, Phydrus: Python implementation of the HYDRUS-1D unsaturated
 606 zone model, Version 0.2.0, available at <https://github.com/phydrus/phydrus> (last access: 30 August 2022)
- 607 Demand, D., and M. Weiler (2021), Potential of a Gravity-Driven Film Flow Model to Predict Infiltration in a
 608 Catchment for Diverse Soil and Land Cover Combinations, *Water Resources Research*, 57(5), e2019WR026988.
 609 <https://doi.org/10.1029/2019WR026988>
- 610

- 611 Germann, P. F., and V. Prasuhn (2018), Viscous Flow Approach to Rapid Infiltration and Drainage in a Weighing
612 Lysimeter, *Vadose Zone Journal*, 17(1), 170020. <https://doi.org/10.2136/vzj2017.01.0020>
- 613 GNIP, Global Network of Isotopes in Precipitation available at <https://www.iaea.org/services/networks/gnip> (last
614 access: 12.02.2023)
- 615 Green, W. H., and G. A. Ampt (1911), Studies in soil physics. 1 The flow of air and water through soils, *J Agric Sci*,
616 4, 1–24.
- 617 Groh, J., C. Stumpp, A. Lücke, T. Pütz, J. Vanderborght, and H. Vereecken (2018), Inverse Estimation of Soil
618 Hydraulic and Transport Parameters of Layered Soils from Water Stable Isotope and Lysimeter Data, *Vadose Zone*
619 *Journal*, 17(1). <https://doi.org/10.2136/vzj2017.09.0168>
- 620 Hansen, S., P. Abrahamsen, C. T. Petersen, and M. Styczen (2012), Daisy: Model Use, Calibration, and Validation,
621 *Transactions of the ASABE*, 55(4), 1317. <https://doi.org/10.13031/2013.42244>
- 622 Harman, C. J. (2015), Time-variable transit time distributions and transport: Theory and application to storage-
623 dependent transport of chloride in a watershed, *Water Resources Research*, 51(1), 1-30.
624 <https://doi.org/10.1002/2014WR015707>
- 625 Heidbüchel, I., J. Yang, A. Musolff, P. Troch, T. Ferré, and J. H. Fleckenstein (2020), On the shape of forward
626 transit time distributions in low-order catchments, *Hydrol. Earth Syst. Sci.*, 24(6), 2895-2920.
627 <https://doi.org/10.5194/hess-24-2895-2020>
- 628 Heße, F., M. Zink, R. Kumar, L. Samaniego, and S. Attinger (2017), Spatially distributed characterization of soil-
629 moisture dynamics using travel-time distributions, *Hydrol. Earth Syst. Sci.*, 21(1), 549-570.
630 <https://doi.org/10.5194/hess-21-549-2017>
- 631 Hirschi, M., D. Michel, I. Lehner, and S. I. Seneviratne (2017), A site-level comparison of lysimeter and eddy
632 covariance flux measurements of evapotranspiration, *Hydrol. Earth Syst. Sci.*, 21(3), 1809-1825.
633 <https://doi.org/10.5194/hess-21-1809-2017>
- 634 Hrachowitz, M., H. Savenije, T. A. Bogaard, D. Tetzlaff, and C. Soulsby (2013), What can flux tracking teach us
635 about water age distribution patterns and their temporal dynamics?, *Hydrol. Earth Syst. Sci.*, 17(2), 533-564.
636 <https://doi.org/10.5194/hess-17-533-2013>
- 637 Hrachowitz, M., P. Benettin, B. M. van Breukelen, O. Fovet, N. J. K. Howden, L. Ruiz, Y. van der Velde, and A. J.
638 Wade (2016), Transit times—the link between hydrology and water quality at the catchment scale, *Wiley*
639 *Interdisciplinary Reviews: Water*, 3(5), 629-657. <https://doi.org/10.1002/wat2.1155>
- 640 Jing, M., R. Kumar, F. Heße, S. Thober, O. Rakovec, L. Samaniego, and S. Attinger (2020), Assessing the response
641 of groundwater quantity and travel time distribution to 1.5, 2, and 3 °C global warming in a mesoscale central
642 German basin, *Hydrol. Earth Syst. Sci.*, 24(3), 1511-1526. <https://doi.org/10.5194/hess-24-1511-2020>
- 643 Köhne, J. M., S. Köhne, B. P. Mohanty, and J. Šimůnek (2004), Inverse Mobile–Immobile Modeling of Transport
644 During Transient Flow: Effects of Between-Domain Transfer and Initial Water Content, *Vadose Zone Journal*,
645 3(4), 1309-1321. <https://doi.org/10.2113/3.4.1309>
- 646 Kumar, R., et al. (2020), Strong hydroclimatic controls on vulnerability to subsurface nitrate contamination across
647 Europe, *Nature Communications*, 11(1), 6302. <https://doi.org/10.1038/s41467-020-19955-8>
- 648 Kumaraswamy, P. (1980), A generalized probability density function for double-bounded random processes,
649 *Journal of Hydrology*, 46(1), 79-88. [https://doi.org/10.1016/0022-1694\(80\)90036-0](https://doi.org/10.1016/0022-1694(80)90036-0)
- 650 Larsbo, M., and N. Jarvis (2005), Simulating Solute Transport in a Structured Field Soil, *J Environ Qual*, 34(2),
651 621-634. <https://doi.org/10.2134/jeq2005.0621>
- 652 Makkink, G. F. (1957), Testing the Penman formula by means of lysimeters, *Journal of the Institution of Water*
653 *Engineers*, 11(3), 277-288.
- 654 Menzel, L., and N. Demuth (1993), Tracerhydrologische Untersuchungen am Lysimeter Rietholzbach, 24 pp,
655 Geographisches Institut ETH Zürich, Zurich, Switzerland.
- 656 Michel, D., M. Hirschi, and S. I. Seneviratne, Stable water isotopes at Rietholbach lysimeter, Switzerland, available
657 at <https://doi.org/10.3929/ethz-b-> (last access: 3 February 2023)
- 658 Nelson, D. B., D. Basler, and A. Kahmen (2021), Precipitation isotope time series predictions from machine
659 learning applied in Europe, *Proceedings of the National Academy of Sciences*, 118(26), e2024107118.
660 [doi:10.1073/pnas.2024107118](https://doi.org/10.1073/pnas.2024107118)
- 661 Nguyen, T. V., R. Kumar, A. Musolff, S. R. Lutz, F. Sarrazin, S. Attinger, and J. H. Fleckenstein (2022), Disparate
662 Seasonal Nitrate Export From Nested Heterogeneous Subcatchments Revealed With StorAge Selection Functions,
663 *Water Resources Research*, 58(3), e2021WR030797. <https://doi.org/10.1029/2021WR030797>
- 664 Or, D., P. Lehmann, E. Shahraeeni, and N. Shokri (2013), Advances in Soil Evaporation Physics—A Review,
665 *Vadose Zone Journal*, 12(4), vzj2012.0163. <https://doi.org/10.2136/vzj2012.0163>

- 666 Peschke, G. (1985), Zur Bildung und Berechnung von Regenabfluß, *Wissenschaftliche Zeitschrift der Technischen*
667 *Universität Dresden*, 34(4).
- 668 Quelo, P., L. Carraro, P. Benettin, G. Botter, A. Rinaldo, and E. Bertuzzo (2015), Transport of fluorobenzoate
669 tracers in a vegetated hydrologic control volume: 2. Theoretical inferences and modeling, *Water Resources*
670 *Research*, 51(4), 2793-2806. <https://doi.org/10.1002/2014WR016508>
- 671 Richter, D. (1995), Ergebnisse methodischer Untersuchungen zur Korrektur des systematischen Meßfehlers des
672 Hellmann-Niederschlagsmessers, Selbstverlag des Deutschen Wetterdienstes, Offenbach am Main.
- 673 Rigon, R., and M. Bancheri (2021), On the relations between the hydrological dynamical systems of water budget,
674 travel time, response time and tracer concentrations, *Hydrological Processes*, 35(1), e14007.
675 <https://doi.org/10.1002/hyp.14007>
- 676 Rinaldo, A., P. Benettin, C. J. Harman, M. Hrachowitz, K. J. McGuire, Y. van der Velde, E. Bertuzzo, and G. Botter
677 (2015), Storage selection functions: A coherent framework for quantifying how catchments store and release water
678 and solutes, *Water Resources Research*, 51(6), 4840-4847. <https://doi.org/10.1002/2015WR017273>
- 679 Saltelli, A., M. Ratto, T. Andres, F. Campolongo, J. Cariboni, D. Gatelli, M. Saisana, and S. Tarantola (2008),
680 *Global Sensitivity Analysis. The Primer*, John Wiley & Sons, Ltd, Chichester, England.
- 681 Salvucci, G. D. (1993), An approximate solution for steady vertical flux of moisture through an unsaturated
682 homogeneous soil, *Water Resources Research*, 29(11), 3749-3753. <https://doi.org/10.1029/93wr02068>
- 683 Schwemmler, R., Roger - a process-based hydrologic toolbox in Python, available at [https://github.com/Hydrology-](https://github.com/Hydrology-IFH/roger)
684 [IFH/roger](https://github.com/Hydrology-IFH/roger) (last access: 20 January 2023)
- 685 Seeger, S., and M. Weiler (2014), Reevaluation of transit time distributions, mean transit times and their relation to
686 catchment topography, *Hydrol. Earth Syst. Sci.*, 18(12), 4751-4771. <https://doi.org/10.5194/hess-18-4751-2014>
- 687 Seneviratne, S. I., et al., Swiss prealpine Rietholzbach research catchment and lysimeter: 32 year time series and
688 2003 drought event, available at <https://doi.org/10.3929/ethz-b-> (last access: 3 February 2023)
- 689 Seneviratne, S. I., et al. (2012b), Swiss prealpine Rietholzbach research catchment and lysimeter: 32 year time series
690 and 2003 drought event, *Water Resources Research*, 48(6). <https://doi.org/10.1029/2011wr011749>
- 691 Šimůnek, J., M. T. van Genuchten, and M. Šejna (2016), Recent Developments and Applications of the HYDRUS
692 Computer Software Packages, *Vadose Zone Journal*, 15(7), v2016.2004.0033.
693 <https://doi.org/10.2136/vzj2016.04.0033>
- 694 Sprenger, M., S. Seeger, T. Blume, and M. Weiler (2016), Travel times in the vadose zone: Variability in space and
695 time, *Water Resources Research*, 52(8), 5727-5754. <https://doi.org/10.1002/2015WR018077>
- 696 Sprenger, M., et al. (2019), The Demographics of Water: A Review of Water Ages in the Critical Zone, *Reviews of*
697 *Geophysics*, 57(3), 800-834. <https://doi.org/10.1029/2018rg000633>
- 698 Steinbrich, A., H. Leister, and M. Weiler (2016), Model-based quantification of runoff generation processes at high
699 spatial and temporal resolution, *Environmental Earth Sciences*, 75(21), 1423. [https://doi.org/10.1007/s12665-016-](https://doi.org/10.1007/s12665-016-6234-9)
700 [6234-9](https://doi.org/10.1007/s12665-016-6234-9)
- 701 Sternagel, A., R. Loritz, W. Wilcke, and E. Zehe (2019), Simulating preferential soil water flow and tracer transport
702 using the Lagrangian Soil Water and Solute Transport Model, *Hydrol. Earth Syst. Sci.*, 23(10), 4249-4267.
703 <https://doi.org/10.5194/hess-23-4249-2019>
- 704 Sternagel, A., R. Loritz, B. Berkowitz, and E. Zehe (2022), Stepping beyond perfectly mixed conditions in soil
705 hydrological modelling using a Lagrangian approach, *Hydrol. Earth Syst. Sci.*, 26(6), 1615-1629.
706 <https://doi.org/10.5194/hess-26-1615-2022>
- 707 van der Velde, Y., P. J. J. F. Torfs, S. E. A. T. M. van der Zee, and R. Uijlenhoet (2012), Quantifying catchment-
708 scale mixing and its effect on time-varying travel time distributions, *Water Resources Research*, 48(6).
709 <https://doi.org/10.1029/2011WR011310>
- 710 Weiler, M. (2005), An infiltration model based on flow variability in macropores: development, sensitivity analysis
711 and applications, *Journal of Hydrology*, 310(1), 294-315. <https://doi.org/10.1016/j.jhydrol.2005.01.010>
- 712 Weiler, M., and F. Naef (2003), An experimental tracer study of the role of macropores in infiltration in grassland
713 soils, *Hydrological Processes*, 17(2), 477-493. <https://doi.org/10.1002/hyp.1136>
- 714 Wilusz, D. C., C. J. Harman, W. P. Ball, R. M. Maxwell, and A. R. Buda (2020), Using Particle Tracking to
715 Understand Flow Paths, Age Distributions, and the Paradoxical Origins of the Inverse Storage Effect in an
716 Experimental Catchment, *Water Resources Research*, 56(4), e2019WR025140.
717 <https://doi.org/10.1029/2019WR025140>
- 718 Yang, X., S. Jomaa, and M. Rode (2019), Sensitivity Analysis of Fully Distributed Parameterization Reveals
719 Insights Into Heterogeneous Catchment Responses for Water Quality Modeling, *Water Resources Research*,
720 55(12), 10935-10953. <https://doi.org/10.1029/2019wr025575>
- 721